Environmental Modelling and Software 179 (2024) 106117

Contents lists available at ScienceDirect

Environmental Modelling and Software

journal homepage: www.elsevier.com/locate/envsoft

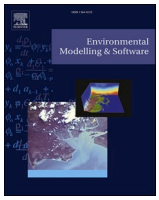

Hydrodynamic modeling of floodplains with inundated trees and floating plants

Wencai Zhou [a,*], John M. Melack [a,b,c], Sally MacIntyre [a,c]

[a] Earth Research Institute, University of California, Santa Barbara, California, USA
[b] Bren School of Environmental Science and Management, University of California, Santa Barbara, California, USA
[c] Department of Ecology, Evolution and Marine Biology, University of California, Santa Barbara, California, USA

ARTICLE INFO

Keywords:
Aquatic vegetation
Floodplains
Drag
Lateral exchange
Thermal structure

ABSTRACT

Hydrodynamic influences of inundated forests and floating plants, common on floodplains, include modifying exchange flows and thermal structure. This study added algorithms to represent these plants in a three-dimensional hydrodynamic model, applied the model to a tropical floodplain, and validated the results with high resolution field measurements. The simulations reproduced temporal and spatial variation of thermal structures in vegetated and open water areas and demonstrated that vertical and horizontal temperature gradients were enhanced in the presence of vegetation. The study extends research findings obtained from laboratory experiments to in-situ situations and to vegetation not represented in the laboratory. The results are relevant to lateral and vertical exchanges of dissolved gases and solutes, and indicate that loss of inundated forests could lead to enhanced lateral exchange.

1. Software availability

The AEM3D model used for the hydrodynamic simulations was obtained from HydroNumerics (Dallimore, 2019). According to the policy of HydroNumerics, source code can be provided to users who can make contributions to the model development; a version with full capacity can be purchased from HydroNumerics under a single-user license. A demo version of the model is available at https://www.hydronumerics.com.au/software/aquatic-ecosystem-model-3d.

2. Introduction

Lakes often contain aquatic plants that modify flow due to their drag (Nepf, 1999; Nakayama et al., 2020). In particular, the increased drag may lead to reduced exchange between vegetated areas and open waters, with implications for fluxes of pollutants and nutrients and provision of habitat for organisms. To understand the key driving variables for increased drag, laboratory experiments have been conducted including ones that modified arrangement and number of rigid cylinders, (Zhang and Nepf 2008; Sanjou et al., 2017; Shan et al., 2019). Laboratory experiments using porous obstructions have illustrated the influence of rooted aquatic vegetation on density-driven exchange flows (Zhang and Nepf 2009, 2011). Empirical relations have quantified the bulk drag coefficient for emergent rigid vegetation (Kothyari et al., 2009). Studies of drag forces with tidal flows over seagrass beds (Monismith et al., 2019) and kelp forests (Monismith et al., 2022) provide estimates of drag based on velocity and pressure measurements for flexible, submerged plants and algae. Results from the laboratory experiments and field measurements, and the resultant equations, are relevant for developing procedures to compute drag in hydrodynamical models used for lakes, including in the extensive flooded forests and floating meadows of floodplain lakes found in many regions of the world.

Aquatic plants can also modify the extent of heating or cooling, with the potential to moderate exchange flows. Due to shading by floating and emergent vegetation, differential heating can occur as the vegetated part of water absorbs less solar radiation than the adjacent open water. As a consequence, warmer near-surface water flows to the vegetated region and cooler water flows beneath back to the open water region, as demonstrated in field investigations (Pokorny and Kvet, 2004; Lovestedt and Bengtsson, 2008) and laboratory experiments (Coates and Patterson, 1993; Coates and Ferris, 1994). However, the case in which absorption of heat in the near-surface water among the plants exceeds the effect of their shading has not previously been examined.

* Corresponding author.
E-mail address: wencaizhou@ucsb.edu (W. Zhou).

https://doi.org/10.1016/j.envsoft.2024.106117
Received 3 April 2024; Received in revised form 22 May 2024; Accepted 3 June 2024
Available online 16 June 2024

Although laboratory experiments provide valuable insights, there remain significant differences between natural vegetation in lakes and wetlands and vegetation configurations used in laboratory experiments. For example, the diameter of trees in inundated forests is non-uniform and diameters are larger (Pangala et al., 2017), and the abundance of floating plants is usually greater than represented in the laboratory. A solution is to use three-dimensional (3D) hydrodynamic modeling, informed with results of experiments, and incorporating natural vegetation and relevant meteorological and limnological conditions. Models need to include the influence of several types of aquatic vegetation on drag and on differential heating or cooling.

Modeling circulation and exchange flows is particularly challenging in floodplains, an aquatic environment found worldwide, that have variable vegetation and depths of inundation. Whether the vegetation is submerged or emergent varies with water level, and floating plants can be prevalent. Additional complexity arises when flows are into and out of an embayment with vegetation along the margins with forces external to the embayment contributing to flow. Results from modeling these environments are especially relevant to ecosystem function, such as productivity, and pollutant dispersion.

The purpose of this paper is to examine hydrodynamic processes in inundated forests and floating plants through 3D modeling evaluated with high-resolution field measurements. To do so required modification of a 3D hydrodynamic model to include influences of aquatic vegetation on drag and differential heating or cooling. Effects of extent and type of vegetation, and varied wind fields, on lateral exchange and thermal structure were examined through a series of experimental simulations. Specific objectives include: 1) incorporating hydrodynamic influences of inundated forests and floating plants in a 3D hydrodynamic model, 2) evaluating the performance of the modified model's ability to simulate thermal structure compared to field measurements, in open water, within inundated forests and under floating plants, 3) simulating lateral exchanges among vegetated areas and open water, 4) comparing results reported in laboratory experiments with natural conditions, and 5) consideration of how modifications of aquatic vegetation could alter limnological conditions.

3. Methods

3.1. Model description

Numerical simulations were done using the Aquatic Ecosystem Model 3D (AEM3D) (Hodges and Dallimore 2019). The model is a coupled 3D hydrodynamic-ecosystem model, of which only the hydrodynamic module was used in this study. This module is based on a hydrodynamic model previously known as Estuary, Lake and Coastal Ocean Model (ELCOM) and uses a z-coordinate Cartesian grid allowing non-uniform spacing in three directions and solves the unsteady Reynolds-averaged Navier-Stokes equation under the Boussinesq approximation (Hodges et al., 2000). The numerical scheme is a semi-implicit finite difference method solving 3D shallow-water momentum equations for stratified flows, adopted from TRIM-3D (Casulli and Cheng 1992) with modification. Temperature is modeled with the ULTIMATE and the QUICKEST methods for scalar transport (Leonard 1991). Turbulence in horizontal and vertical is characterized by an eddy-viscosity method (Hodges and Dallimore 2019) and an energy budget method for mixing (Imberger and Patterson, 1981; Spigel et al., 1986), respectively.

3.2. Representing vegetation in model

Incorporation of hydrodynamic influences of inundated forests and floating plants required adding new algorithms and other modifications to AEM3D.

The bulk drag coefficient (C_D) imposed by inundated forests was calculated following Kothyari et al. (2009) in which forests are considered rigid stems extending through the whole water column:

$$C_D = 1.8\xi R_d^{-\frac{3}{50}}[1 + 0.45\ln(1 + 100\lambda)]\left(0.8 + 0.2F - 0.15F^2\right) \quad (1)$$

With λ, the cross-sectional area of trees per unit bed area:

$$\lambda = \frac{n\pi d^2}{4A} \quad (2)$$

R_d , the stem Reynolds number:

$$R_d = \frac{V_c d}{\nu} \quad (3)$$

F , the Froude number:

$$F = \frac{V_c}{\sqrt{gh}} \quad (4)$$

Where, n is the number of trees, A the area of study site (m^2), d the tree diameter (m), V_c depth-averaged flow velocity (m s^{-1}), ν kinematic viscosity of water (m^2 s^{-1}), g gravitational acceleration (m s^{-2}), h water depth (m) and ξ a staggering pattern parameter (dimensionless).

The vertical distribution of vegetation drag for rooted emergent trees is calculated from bottom to surface as:

$$C_{Di} = C_D\frac{\Delta l_i}{\Delta z_i} \quad (5)$$

where C_{Di} is the drag coefficient of the ith layer, Δz_i the thickness of the ith layer and Δl_i the length of tree stem in the ith layer. The vertical extent of the tree is bottom referenced.

The vertical extension of floating plants is specified as the depth to which the plant stems and roots reach. Hence, the vertical profile of vegetation drag is also calculated following Eq. (5) but from surface downward and is top referenced.

3.3. Model preparation

Most of the model parameters were configured with default non-site-specific literature values as suggested by Hodges and Dallimore (2019) (Table 1), except that k_d was based on measured profiles of irradiance, and attenuation coefficients for ultraviolent radiation and five wavelength bands of near-infrared radiation were adopted from Jellison and Melack (1993). The bulk transfer coefficients for heat and momentum

Table 1
Key parameters used for the AEM3D simulations.

Parameter		Value	Unit
Mixing coefficients	Wind stirring	1.33	–
	Shear generation of turbulent kinetic energy (TKE)	0.15	–
	Convection	0.2	–
	Bottom generation of TKE	2.2	–
	Dissipation of excess energy	1.15	–
Attenuation coefficients	PAR	1.8 (field data)	m^{-1}
	UVA	1.0	m^{-1}
	UVB	2.5	m^{-1}
	NIR, 700–800 nm	1.1	m^{-1}
	NIR, 800–900 nm	3.4	m^{-1}
	NIR, 900–1000 nm	26	m^{-1}
	NIR, 1200–1800 nm	870	m^{-1}
	NIR, 1800–2800 nm	7800	m^{-1}
Bulk transfer coefficients	Heat	0.0013	–
	Momentum	0.0013	–
Mean albedo	Shortwave radiation	0.08	–
	Longwave radiation	0.03	–
Bulk drag coefficient for vegetation	Flooded forest	1.0	–
	Floating plants	10.0	–
Bottom drag coefficient		0.0035	–

were initialized using customized values (Table 1) and then corrected by AEM3D during the simulations to account for effects of non-neutral atmospheric stability. AEM3D was configured with the domain discretized into 5 × 5 m mesh grids in the horizontal and 0.1 m layers in the vertical and a simulation time step of 20 s.

C_D in the inundated forest was estimated in five steps. 1) λ was obtained from field measurements of tree size and number near the embayment in Janauacá (Pangala et al., 2017). Diameter of young trees (d_1) and mature trees (d_2) at breast height was below 0.06 m and between 0.06 and 0.74 m, respectively; the number of young trees (n_1) and mature trees (n_2) was 244 and 436, respectively, in a 50 × 80 m plot (A = 4000 m^2). λ was calculated with three scenarios: all trees were young trees of 0.06 m in diameter, all trees were mature trees of 0.74 m in diameter, and all trees are of averaged diameter $(n_1d_1 + n_2d_2)/(n_1 + n_2)$. 2). Kinematic viscosity of water ν was calculated as a function of temperature which ranged from 28 °C to 36 °C following Batchelor (1967). 3) Depth-averaged flow velocity V_c was assumed to vary from 0.005 m s^{-1} to 0.1 m s^{-1}, based on measurements with an acoustic Doppler velocity sensor (MacIntyre et al., 2019). 4) A water depth of 1.0 m was used, based on measurements at time of simulations, 5) A triangular-staggering pattern ($\xi = 1$) was used because it represents the distribution of trees better than a regular-square staggering pattern (Kothyari et al., 2009).

Vegetation height for inundated forest was set to be from bottom of the embayment to 4 m above the water surface, and vegetation height for floating plants was set to −0.3 m (the upper most 0.3 m of the water column). The vegetation height for inundated forest is not critical if the tree canopy is above water surface.

Given that the velocity in the open water was negligible to 0.1 m s^{-1}, supercritical flows (Froude number $F > 1$) would only be found at locations where the depth was less than 0.001 m, hence it is reasonable to assume the flow in the inundated forest was subcritical. Under all three scenarios of trees and within the given ranges of T and V_c, C_D decreased from around 1.5 at the low temperature and low flow velocity end to slightly below 1.0 as either temperature or flow velocity increased within the given ranges (Fig. S1). Thus, it is reasonable to set the bulk drag coefficient in inundated forest as 1.0.

Floating plants on Amazon floodplains attain high biomass with most underwater and with the numbers of stems with roots averaging 70 m^{-2} (Engle et al., 2008). Hence, given the much higher vegetation density for submerged portions of floating plants than flooded forest, the vegetation drag was set to 10.

Meteorological data required as model inputs for regions with open water and floating plants were measured (Fig. S2). For the inundated forest, incoming shortwave radiation was reduced by 70% and wind speed by 50% based on comparative measurements in inundated forests and nearby open water in similar locations. To mimic the thermodynamic behavior of water around floating plants, shortwave albedo was reduced by 40% and the diffuse attenuation coefficient was set to 18 m^{-1}, which was 10 times the value in open water (Table 1) and produced about 0.3 m as the depth of 1% light penetration (roughly the depth of diurnal thermocline) in floating plants.

3.4. Experimental simulations

Five experimental simulations were done by varying combinations of vegetation, and wind speed and direction (Table 2) to examine effects of extent and type of vegetation, and varied wind fields, on lateral exchange and thermal structure. Simulations s1 to s3 were designed to address the impacts of inundated forests and floating plants; simulation s4 examined impacts of different wind directions, and simulation s5 added internal waves driven by temperature profiles from outside the embayment (Text S2). For simulation s4 and s5, increased wind speed and altered wind direction along the main axis of the embayment were adopted for two reasons. First, the wind station was installed close to flooded forest at the northeastern end of the embayment, which may have reduced wind speed due to the sheltering by the trees. Second, elevated wind speed during daytime likely came from the southwest given that the wind station was surrounded by trees from three directions and open to the southwestern direction.

Table 2
Experimental AEM3D simulations.

Simulations	Vegetation		Wind data	
	Flooded forest	Floating plants	Wind speed (m s^{-1})	Wind direction
s1	+	+	Field data	Northeast
s2	+	–	Field data	Northeast
s3	–	–	Field data	Northeast
s4	+	+	Field data	Southwest
s5$^+$	+	+	Field data × 1.5	Southwest

$^+$Boundary condition added to capture influence of internal waves generated outside the basin.

3.5. Model performance

To evaluate the performance of the modified AEM3D model, root mean square error (*RMSE*) and percent relative error (*PRE*) were computed to examine the absolute and relative deviation of the simulated results to the measured data. Correlation coefficients (R) were used to examine how well the variation of simulated results match with the measured data. The three statistics were computed as follows:

Root mean square error (*RMSE*)

$$RMSE = \sqrt{\frac{\sum_{i=1}^{n}(S_i - O_i)^2}{n}} \tag{6}$$

Percent relative error (*PRE*)

$$PRE = \frac{\sum_{i=1}^{n}(S_i - O_i)/O_i}{n} * 100 \tag{7}$$

Correlation coefficient (R)

$$R = \frac{\sum_{i=1}^{n}(S_i - \overline{S})(O_i - \overline{O})}{\sqrt{\sum_{i=1}^{n}(S_i - \overline{S})^2 \sum_{i=1}^{n}(O_i - \overline{O})^2}} \tag{8}$$

where S_i and O_i are the 'i-th' simulated and observed data, $\overline{S}$ and $\overline{O}$ the mean simulated and observed data, and n the total number of data points. To ensure the same depth-time coordinates of the simulated and measured data, the simulated temperatures were averaged to 5-min bins and resampled to the depths nearest to the depths of measurements.

Two groups of statistics were computed with the measured and simulated temperature profiles. One computed at each measurement depth with the time series of temperature at that depth: *RMSE, PRE* and R of $T(t)$) examined the model's performance capturing the temporal variation of temperature. The other computed at each time of measurement with the temperature over all the depths: *RMSE, PRE* and R of $T(z)$) evaluated the model's performance capturing vertical variations of temperature.

3.6. Study site

The modified hydrodynamic model was applied to a floodplain lake in the central Amazon basin (Brazil) (Fig. 1a) with the three major floodplain environments, open water, inundated trees, and floating plants (Hess et al., 2015). Here, we focus on a period of high water to evaluate the model's performance. More information about the study site is provided in Amaral et al. (2018; 2021) and Barbosa et al. (2020).

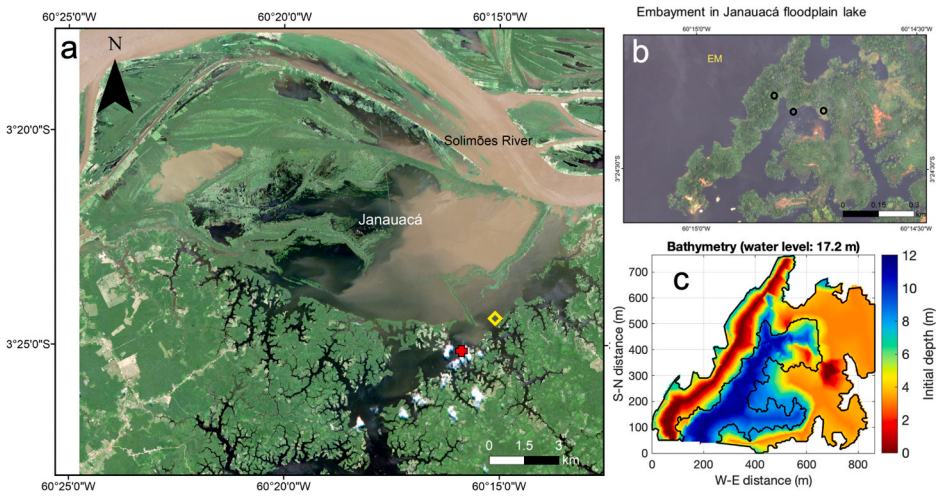

Fig. 1. Satellite images of Lake Janauacá (3.38°S, 60.3°W) (a), an embayment (b), and topographic and bathymetric data for the embayment (c). Locations of embayment (yellow diamond) and water level gauges (red cross) are marked in panel a; locations of moored thermistors in inundated forest, open water and floating plants are marked as black circles from left to right in panel b.

3.7. Field measurements

The bathymetry is based on data collected in open water during high water periods using echo sounders and manual measurements of depths in flooded forest. A digital elevation map was prepared using methods described in Rudorff et al. (2014). Perimeters of the flooded forest and floating plants were determined from a satellite image (Apollo World View −2 image on 08/14/2014).

Temperature sensors were deployed in each habitat on taut-line moorings combined with additional sensors below surface floats. The uppermost sensor is attached to the base of the surface float to obtain surface water temperature at ~0.05 m. RBR Solo® thermistors (accuracy 0.002 °C) sampled at 0.1 Hz. The thermistors were spaced about 0.25 m apart in the upper 1 m and about 0.5–1 m below 2 m. Wind speed and direction sensors were deployed 2 m above the water surface on a buoy at the open water site. Measurements of incoming shortwave radiation, air temperature, relative humidity 2 m above water surface, rainfall, wind speed and wind direction at both 2 m and 4 m above water surface were also made at a nearby floating research station. Vertical profiles of photosynthetic active radiation (PAR) were obtained using a Licor LI-192 SB underwater sensor, and the diffuse attenuation coefficient ($K_{d\,PAR}$) was computed from the irradiance profiles following Beers Law. Water levels were manually read from a series of leveled stage gauges (Fig. 1a) on a daily basis.

4. Results

Performance of the 3D hydrodynamic model, including the modification for the influence of drag in the flooded forests and floating plants, to simulate thermal structure was evaluated by comparison to field measurements in open water, within inundated forests and under floating plants (section 4.1) and with statistical metrics (section 4.2). The meteorological conditions used for these simulations are described in Text S1 and illustrated in Fig. S2. Further evaluations were made of simulations of lateral exchanges among vegetated areas and open water (section 4.3 and section 4.4). Comparisons of results reported in laboratory experiments with natural conditions and consideration of how modifications of aquatic vegetation could alter limnological conditions are included in the Discussion.

4.1. Measured and simulated thermal structure in three habitats

The thermal structure in open water, inundated forest and floating plants had pronounced diel cycles, but the extent of heating varied depending on the presence and type of vegetation. At the open water site (Fig. 2a), a diurnal thermocline started to form between 0.5 and 1.0 m about an hour after sunrise and deepened to 2 m at mid-day as a result of increased wind speed (Fig. S1c). The diurnal thermocline continued deepening to 3 m or below in the afternoon when cooling started. Though weakened during the cooling hours, stratification was maintained until early morning of the next day. Variation of thermal structure in flooded forest was similar to that in open water (Fig. 2c), and both showed signs of internal wave motions as indicated by the fluctuations of the 30 °C isotherm. Temperatures and thermal structure around floating plants differed from those in open water and flooded forest. During the heating hours, surface temperature in floating plants reached about 36–39 °C around mid-day, which was roughly 6–8 °C higher than that at the other two sites. Nighttime surface temperatures at the floating plants were similar to those in open water and flooded forest.

AEM3D simulated the diel variation of thermal structure at the three sites, but simulated higher surface temperatures during both daytime and nighttime in open water (Fig. 2b) and flooded forest than measured (Fig. 2d). In floating plants, the simulated surface temperatures were lower during day but higher during night than measured (Fig. 2f). AEM3D simulated insufficient heating in floating plants. AEM3D also simulated less deepening of the diurnal thermocline, as indicated by the fluctuation of the simulated 31°C isotherm compared to fluctuations of the measured 30 °C isotherm. Hence, the model simulated insufficient vertical mixing by either wind shear or convection. Furthermore, AEM3D did not simulate the internal wave motions at the three habitats as shown by the measured temperatures.

The measured temperatures in the flooded forest site did not reflect fully the influence of shading within flooded forests because the site was only about 15 m from open water. The average temperature difference between the two sites (Fig. 2a and 2c) was small (0.13 °C overall, 0.14 °C at 0.03 m and 0.17 °C at 2.93 m). At sites further within the flooded forest (col. 2 and 3 in Fig. 3a), AEM3D simulated temperature profiles 1–3 °C cooler than those in open water (Fig. 3e and 3f), presumably as a result of shading by the forest.

4.2. Model performance

The ability of AEM3D to model thermal structure was evaluated by *RMSE*, *PRE* and *R* of *T(z)* (temporal variation of temperature at sampling depths) and *T(t)* (vertical variation of temperature at time of stratification ($N_{max} > 20$ cph) (Eqs. (6)–(8)). The evaluation was done based on

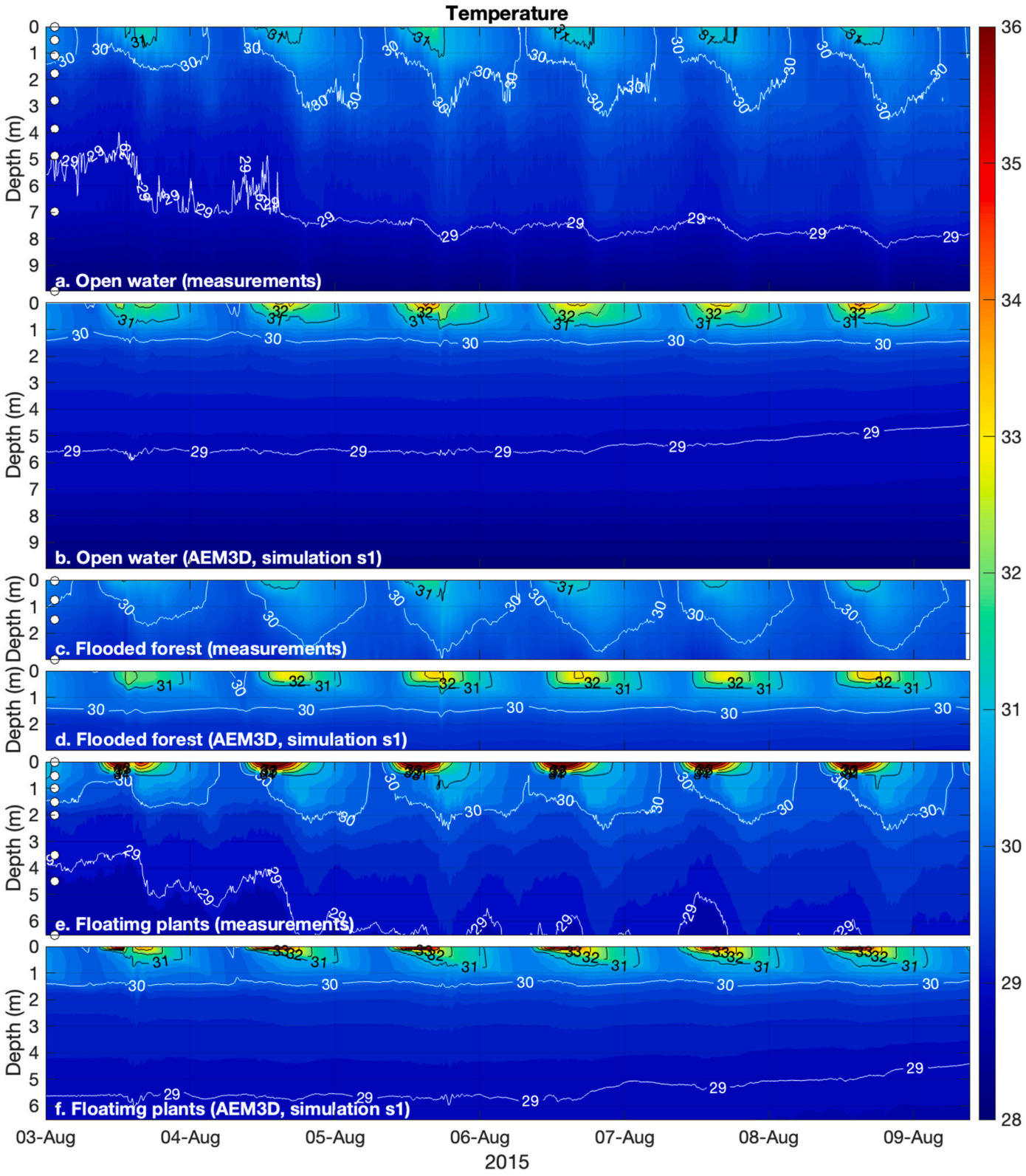

Fig. 2. Measured and simulated temperature (simulation s1) in open water (a and b), flooded forest (c and d) and floating plants (e and f).

simulation s1 (Table 2).

RMSE of *T(z)* showed that absolute deviation at all three habitats decreased from between 1 °C (flooded forest) and 1.2 °C (floating plants) at surface to less than 0.5 °C below 1 m (Fig. 4a$_1$). *PRE* of *T(z)* decreased from between −1% (floating plants) and 3% (open water) at surface to between −1.5% and 0% below 1 m (Fig. 4b$_1$), and the *R* of *T(z)* decreased from above 0.9 to ~0.6 within the upper 1 m (Fig. 4c$_1$). The high values of *RMSE*, *PRE* and *R* of *T(z)* were calculated at depths above the diurnal thermocline where variation of temperature was high (3–9 °C between mid-day and mid-night, Fig. 2), and low values of the three statistics were calculated mostly below the diurnal thermocline where variation of temperature was low (less than 0.5 °C between mid-

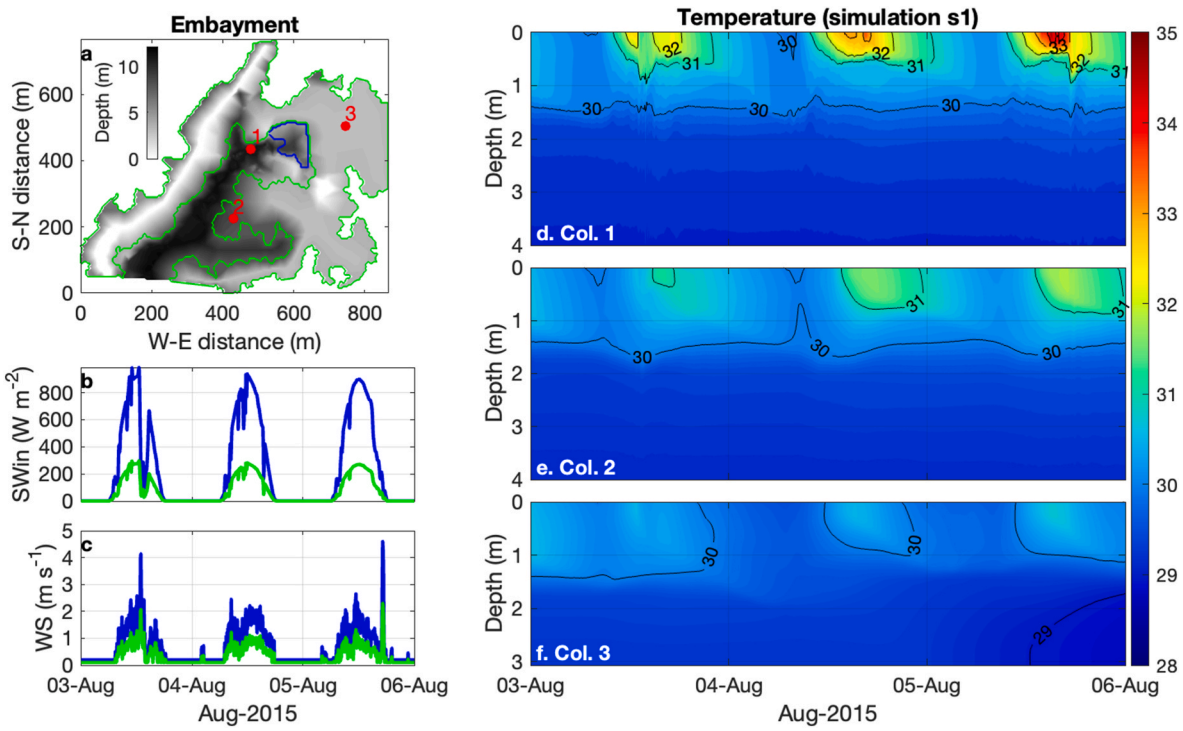

Fig. 3. AEM3D simulated spatial variation of the temperature profiles: a – bathymetry of the embayment and location of temperature profiles shown in panels d to f (red dots and numbers), with green line marking the area of flooded forest, blue line marking the area of floating plants; b – incoming shortwave radiation at open water, floating plants (blue) and flooded forest (green); c – wind speed at open water, floating plants (blue) and flooded forest (green); d – temperature profile at location 1 (open water) shown in panel a; e & f – temperature profile at location 2 and 3 (flooded forest) shown in panel a.

day and mid-night). In particular, *PRE* of *T(z)* (Fig. 4b$_1$) was positive in the upper 1 m and negative below 1 m, showing that AEM3D slightly overestimated temperature near surface and underestimated temperature in the interior of the water column.

RMSE, *PRE* and *R* of *T(t)* showed similar patterns among the three habitats as those of *T(z)*. *RMSE* of *T(t)* varied between peaks from 0.7 to 1.5 °C around mid-day when the water columns at the three habitats were most stratified to lows less than 0.5 °C at sunrise and sunset (Fig. 4a$_2$). *PRE* of *T(t)* varied between −2% and 2%, with relatively high values around mid-day and values close to zero around sunrise and sunset (Fig. 4b$_2$). Values of *PRE* in open water and flooded forest sites were mostly positive, and values in floating plants were mostly negative. Given the variation of *RMSE*, AEM3D simulated stronger vertical stratification in open water and flooded forest while reduced vertical stratification in floating plants, compared to measurements. *R* of *T(t)* was generally greater than 0.8 in all three habitats (Fig. 4c$_2$), indicating that the model simulated the vertical variation of thermal structure well.

4.3. *Effects of flooded forest and floating plants on thermal structure and circulation*

To explore the effects of vegetation on temperature, thermal structure, and exchange flows, simulations were run in which both flooded forest and floating meadows were included (simulation s1, Table 2), only flooded forest was included (simulation s2, Table 2), and when no vegetation was present (simulation s3, Table 2). These simulations were configured with wind speed and direction measured at the open water site and thus did not include weakening of wind speed or solar radiation as when flooded forest was included. Simulated temperatures along a cross-section showed that the presence of vegetation led to higher temperature in the upper part of water column and hence stronger stratification in both open water and vegetated sites (Fig. 5a$_1$ to 5a$_3$ and Fig. 6a$_1$ to 6a$_3$).

Floating plants modulated thermal structure both horizontally and vertically during daytime (Fig. 5a$_1$ and 5a$_2$). In the floating plant beds, simulated water temperatures were 4–6 °C higher than those in the open water and flooded forests. Thus, the floating plants were a heat source to open water, and near-surface water temperatures in adjacent open water were about 0.5–1.0 °C higher than when the plants were not present, indicating the flow of water via a process known as differential heating. In the flooded forest to the east of the floating plants, simulated surface velocities were about 0.2 cm s^{-1} (Fig. 5b$_1$), roughly 0.05 cm s^{-1} higher than when floating plants were not included (Fig. 5b$_2$), indicating that the horizontal velocities in flooded forest were enhanced by the strong horizontal temperature gradient in the presence of floating plants. The floating plants also moderated the depth of the diurnal thermocline. The simulated diurnal thermocline below the plants was half the depth of that in open water. At night, the simulated thermal structure and velocity field with both types of vegetation and those with flooded forest only were similar, indicating that the hydrodynamic impact of floating plants at night was low. In short, the floating plants led to temperature gradients that contributed to exchanges between open water and flooded forest.

In the simulations with progressively less coverage of floating plants and forest, the fetch of the wind progressively increased from 150 m, to 240 m, and to nearly 520 m. With short fetch, higher velocities are only found in the region without plants and have magnitude between 2 and 4 cm s^{-1} in the upper half meter and 2 cm s^{-1} in the next half meter. As discussed above, some of these flows may have been due to horizontal differences in temperature. Without floating plants, the region with elevated velocities increased in the horizontal. These first two cases show a slight tilting of the diurnal thermocline with downwelling to the west as expected for the easterly winds that occurred that day. Without the floating meadow and flooded forest, the thermocline tilting is large enough that the pool of warmer water to the west extends about half way along the width of the embayment and cooler water is upwelled to the east. With greater mixing associated with greater shear from enhanced thermocline tilting, the near-surface waters are cooler and shallower

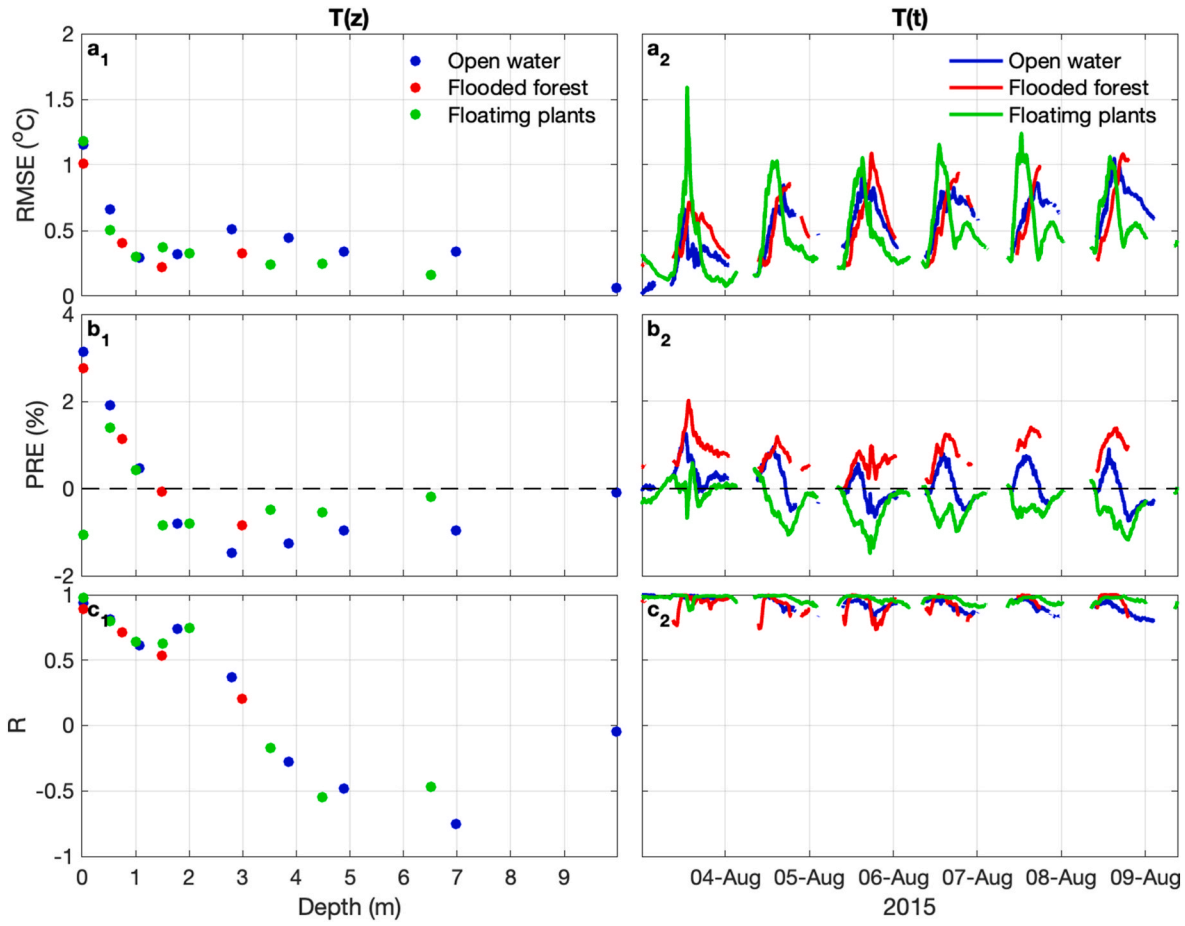

Fig. 4. AEM3D model performance (s1, Table 2): *RMSE, PRE* and *R* of *T(z)* (a_1 to c_1) and *T(t)* (a_2 to c_2) in open water (blue), flooded forest (red) and floating plants (green).

than when plants are present with some of the heat mixed downwards. Flow speeds were minimal below 2 m when the vegetation was present and progressively increased in magnitude below that depth with the loss of vegetative cover. With the greater accumulation of heat during the day when vegetation was present, the simulations indicate that stratification persisted at night (Fig. 6a_1 and 6a_2). However, without vegetation, little heat was retained at night and stratification was minimal (Fig. 6a_3).

4.4. *Thermal structure and flow in the three habitats with changes in wind direction and externally forced internal waves*

Changes in wind direction along the main axis of the embayment lead to upwelling at the back of the embayment and accumulation of heat downwind for a northeasterly wind and downwelling and only a slightly increased accumulation of heat downwind for a southwesterly wind (Fig. 7). The shifts in surface velocity are as to be expected for such winds, that is southerly currents for the northeasterly winds and northerly currents for the southwesterly wind. These are accentuated in the upper 0.3 m with a return flow immediately below. Simulations along a cross-section towards the back of the embayment show greater downwelling to the west with the northeasterly wind and to the east with the southeasterly wind. When internal waves are forced in the basin and the winds are southwesterly and increased by 50%, patterns are similar but with less accumulation of heat most likely due to the enhanced shear and mixing from greater tilting of the diurnal thermocline (Fig. 7c).

While wind speed and direction made a large contribution to flow, the simulations showed that flows were still driven by floating vegetation when present. That is, the horizontal velocities at the surface in floating plants were always towards open water on the west indicating that the temperature gradient was sufficiently strong to overcome the southwest wind (Fig. 8b_2), at least in a region near the plants.

Currents were simulated below the near-surface horizontal circulation. Currents in the same direction and in the opposite direction as the near-surface currents along the longitudinal section were simulated between 4 and 8 m and below 8 m, respectively, with velocities less than that of the surface horizontal circulation under southwest wind (Fig. 7b_2). These currents were enhanced as internal waves were excited at the southwest boundary (Fig. 7b_3). Similar advection was simulated along the cross-section under both east and southwest winds (Fig. 8b_1 to 8b_3).

Surface circulation was simulated at night. Near the surface, the horizontal temperature gradient between floating plants and open water established during the day relaxed as wind speed declined after sunset. As a result, near-surface horizontal circulation, as shown by the horizontal velocities along both sections (Figs. S5 and S6), reversed direction during night as compared to the direction during daytime. Below the near-surface circulation, currents formed during daytime changed direction. Along the cross-section, temperatures in the flooded forest to the west decreased to 29 °C (Fig. S6). From this we infer that the currents between 2 and 4 m under northeast wind and those between 2 and 8 m under southwest wind were driven by gravitational flows induced by differential cooling (Fig. S6).

5. Discussion

A 3D hydrodynamic model modified to include inundated forests and

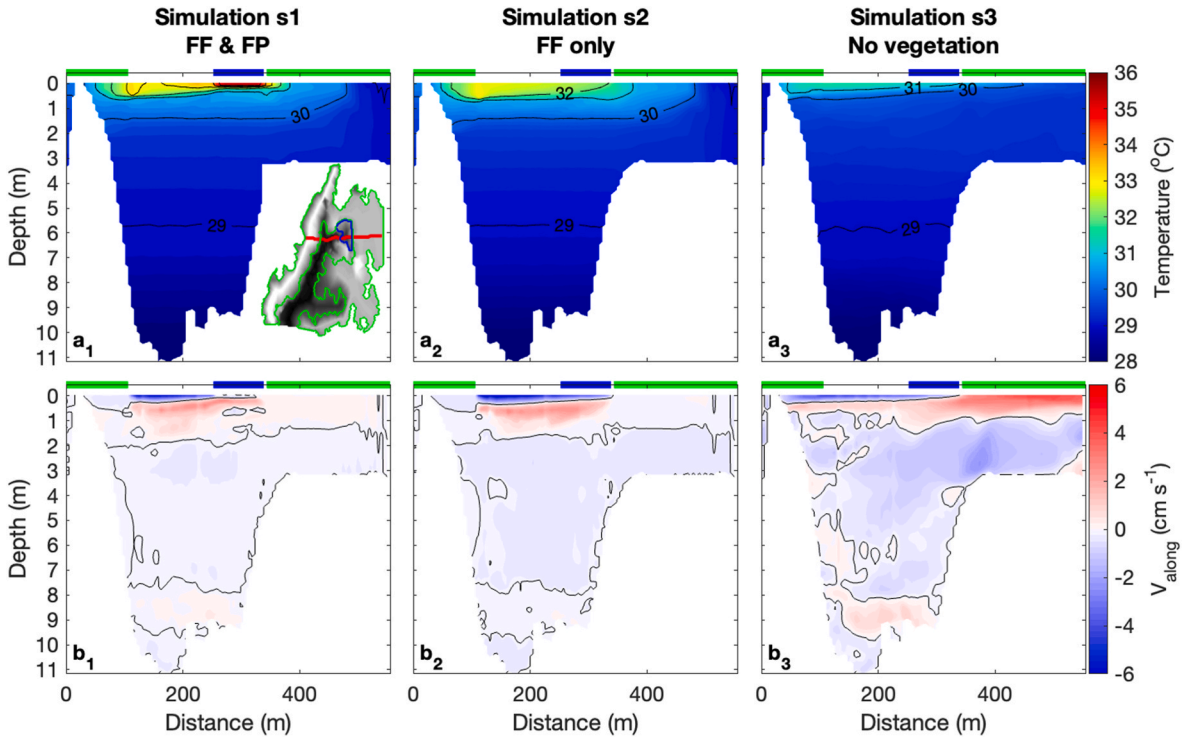

Fig. 5. AEM3D simulated temperatures, and horizontal and vertical velocities along cross-section on Aug 4, 2015 at 14:34 (simulations s1, s2 and s3, Table 2). The location and orientation of the cross-section is shown as the red line in the map at the lower right corner of panel a_1. X-axis is the distance starting from the western end of the cross-section. Green and blue bars along the upper edge of each panel mark the area of flooded forest (FF) and floating plants (FP).

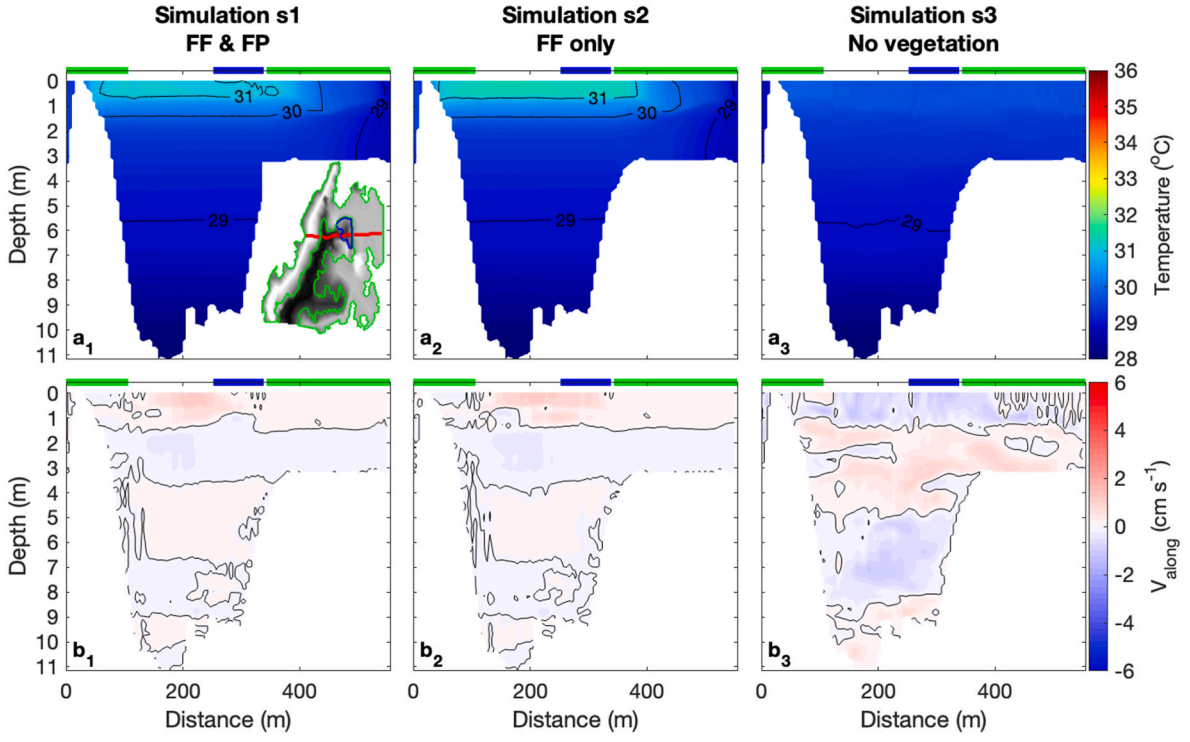

Fig. 6. The same as Fig. 5 but on Aug 5, 2015 at 00:04.

floating plants and driven by field measurements of meteorological and limnological conditions simulated thermal structure well among the vegetated and open water regions. Influences of aquatic vegetation on drag and differential heating or cooling were identified as important processes, and the spatial arrangement and extent of the vegetated regions led to different horizontal velocities, lateral exchange, and thermal structure.

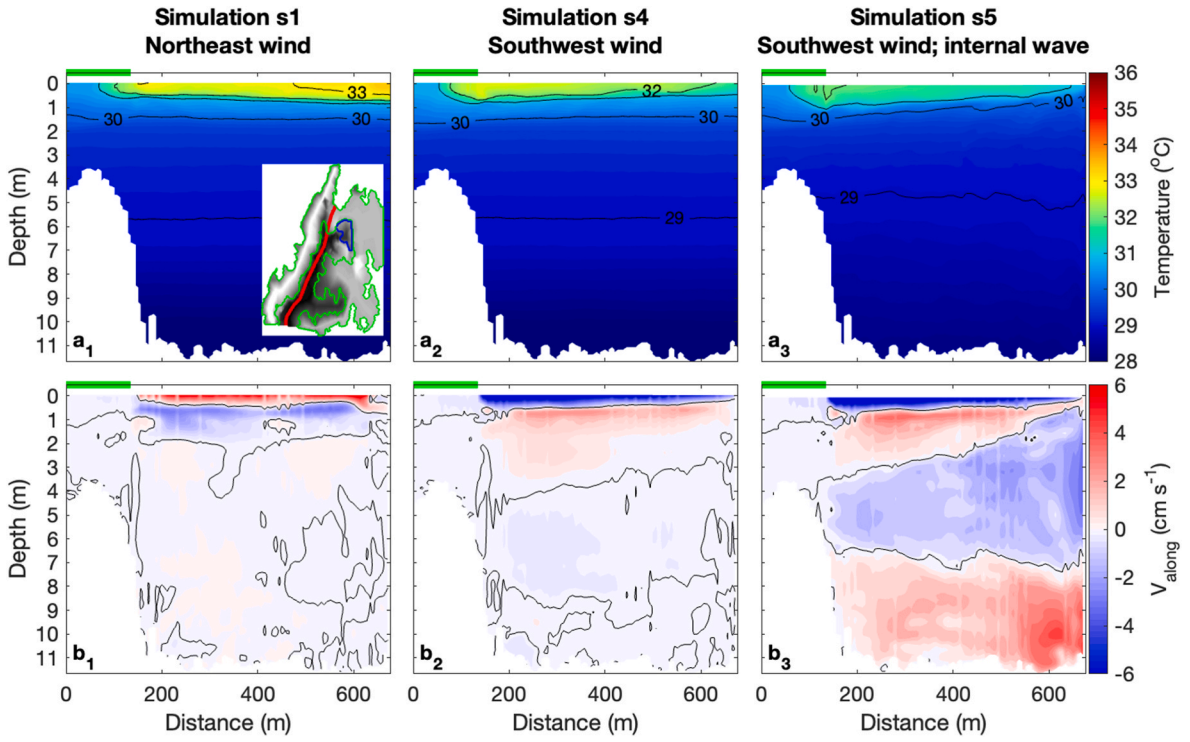

Fig. 7. AEM3D simulated temperatures (a_1 to a_3), and horizontal and vertical velocities (a_1 to a_3) along longitudinal section on Aug 4, 2015 at 14:34 (simulations s1, s4 and s5, Table 2). The location and orientation of the section is shown as the red line in the map at the lower right corner of panel a_1. X-axis shows the distance starting from the northern end of the section. All simulations included flooded forest and floating plants. Section of FF is marked by the green bar along the upper edge of each panel.

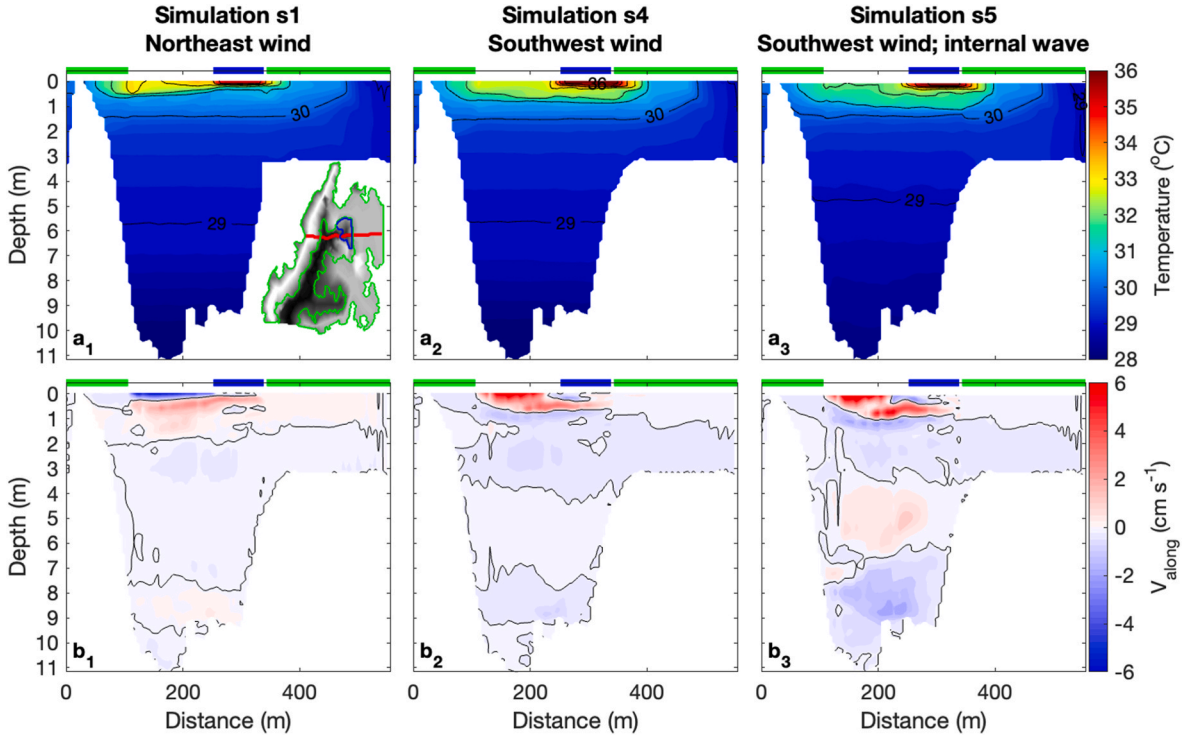

Fig. 8. The same as Fig. 8, but for curtain 3. Sections of FF and FP are marked by the blue and green bars along the upper edge of each panel.

5.1. Extension of laboratory experiments

Gravitational flows when wind speed was low (e.g., Fig. 6) were driven by horizontal temperature gradients (e.g., density differences in the horizontal), similar to laboratory experiments in which the driving force was also a temperature gradient (Zhang and Nepf, 2009) or a salt-derived density gradient (Zhang and Nepf, 2008). When wind speed increased in the embayment, as occurred during the day, the

gravitational flows could be enhanced if wind direction was the opposite to the horizontal temperature gradient (e.g., west of floating plants, Fig. 5a$_1$) or canceled if wind direction was the same as the horizontal temperature gradient (e.g., east of floating plants, Fig. 5a$_1$). The interaction or competition between wind and temperature gradient-induced flows was not characterized in laboratory experiments as wind was not considered in those experiments.

Another difference from laboratory experiments is the nature of the vegetation. In the embayment of Lake Janauacá; tree diameters ranged from 0.06 to 0.74 m with no regular pattern in distance between two adjacent trees. In laboratory experiments (Kothyari et al., 2009), trees were characterized as rigid cylinders less than 0.01 m in diameter, and the cylinders were distributed with regular-square staggered pattern or triangular-staggered pattern. Zhang and Nepf (2011) experimentally modeled the effect of a porous obstruction at the surface of a water body, with the porous obstruction similar to the roots of vegetation. They conducted a lock-exchange experiment, with different densities of water and porosity. Once the gate separating the water with and without the obstruction, they observed two-layer flow below the root bed. In our case, the obstruction is weaker near the surface, where stems and leaves are found, and more pronounced below the surface where the roots occurred. In the experiments higher density water was associated with the roots which were at the surface; in nature, lower density water relative to that in open water was found near the surface of the plant bed and higher density water, relative to that above and at the same depth offshore, was associated with the roots due to the colder temperatures from the shading above. In the field, since the water temperature near the surface exceeded that of the surrounding water in the day, we can infer that the high heat absorption in the near-surface water among the plants exceeded their shading effects. Both field measurements and AEM3D simulations showed that the heat absorbed by and among floating plants can flow to the surrounding water and lead to its increasing in temperature. For the laboratory and field data to be comparable, increased winds in the field would cause flow into the upper part of the floating meadows or into the root mat itself. Our results illustrate larger scale processes of differential heating and cooling as they depend on lake morphometry as in Monismith (1990) and Coates and Patterson (1993).

The timescales of laboratory experiments were much shorter than temperature variation in the field. The AEM3D simulation timestep of 20 s is longer than those using the models based on laboratory experiments of 0.5 s and 0.05 s (Tsakiri and Prinos, 2015; Liu et al., 2017). As a result, AEM3D did not simulate the flow regimes mentioned in Zhang and Nepf (2008, 2009) or the two-layer structure of surface flow in Zhang and Nepf (2011). While the models provide insight into the nature of flow in vegetated environments, our observations better illustrate the influence on the surrounding flow. That is, the pronounced heating among the floating plants drives density driven flows, and the model illustrates how wind driven flows away from the mats are moderated when vegetation is present.

5.2. Potential impacts of deforestation and lack of floating vegeation

AEM3D simulations with and without vegetation indicate potential impacts on floodplains. With flooded forest and floating plants absent, simulations indicated that the stratification between near-surface water and water below diurnal thermocline was reduced by about 2 °C during both day (Fig. 5a$_3$) and night (Fig. 6a$_3$). That is, deforestation would lead to a weakening of stratification as the fetch increased. Lateral exchanges would be enhanced as simulated horizontal velocities in the upper 4 m increased from close to zero when flooded forest was present (Fig. 5b$_2$) to between 2 and 4 cm s^{-1} when flooded forest was removed (Fig. 5b$_3$). With a shorter retention time, solutes or dissolved gases produced would be transported more readily. Additionally, the reduced water movement below the stratified zone when vegetation is present leads to deoxygenation and increases in CH_4 and CO_2. With the weakening of stratification as simulated here, vertical mixing at night may be more effective and reduce the extent of deoxygenation, lead to more oxidation of CH_4 and upward mixing of both CH_4 and CO_2, and increase the available habitat for fish.

Three-dimensional hydrodynamic simulations of conditions in vegetated embayments and nearby open waters are relevant to ecological and biogeochemical understanding in these complex environments. Amaral et al. (2021) illustrated the influence of water motions induced by presence of vegetation, as modeled here, on exchanges of carbon dioxide between the atmosphere and water. That is, the differential cooling induced by cooling in shallow areas (Fig. S4) enables offshore flow of dissolved gases which then can evade to the atmosphere when convective mixing dominates at night. Sharip et al. (2012) reported how density-driven flow induced by differential temperature gradients between regions with floating-leaved or submerged vegetation and open pelagic region in shallow tropical lakes contributed to increased transport of phosphate. Biogeochemical models of the production and atmospheric exchanges of methane, carbon dioxide or oxygen (Tan et al., 2015, 2017) would be improved if such lateral and vertical exchanges were included.

5.3. Challenges of modeling

One challenge was characterization of flooded forest and floating plants in model configurations. The bulk drag coefficient in flooded forest was estimated using empirical equations derived from laboratory experiments with vegetation characterized with smaller diameters and a regular distribution pattern. This method led to a uniform bulk drag coefficient in the flooded forest. That may deviate from reality as the trees varied in both diameter and distribution. Thus there may be varying lateral exchange through the forest. Although the effects of differential absorption among floating plants was simulated, AEM3D was unable to simulate the temperature peaks during the day as the simulated heat loss through latent heat and sensible heat increased with the increasing temperature.

The current model configurations do not characterize the effects of turbulence induced by vegetation on vertical stratification. Such could occur if three dimensional eddies are generated as flow passes tree trunks (Nepf 2012). Capturing that process would require either grid sizes smaller than the tree diameters or quantification of mean vertical turbulent mass flux within each grid. The former is not practical as the tree diameters were too small to be characterized individually by AEM3D, while the latter requires data from field experiments that have not been done.

Another challenge was lack of meteorological data within flooded forests, the location of the wind sensors at one end of the embayment, and the other meteorological sensors nearby but not in the embayment. Rarely would such habitat-specific data be available, and more often models are run with data from land-based meteorological stations or regional data assimilations. Site-specific, on-lake data are likely to improve accuracy of simulations.

When combined with time series temperature measurements, high quality validation can be done to improve simulations. For example, we further improved the model by approximating the influence of internal waves driven by winds at the outer end of the embayment by modifying our lateral boundary conditions. Since AEM3D does not incorporate a mechanism to generate momentum transport across open boundary, it is unable to properly characterize such internal wave motions observed in the embayment. As illustrated in Fig. S4, our approach led to considerable improvement in simulating thermal structure.

6. Conclusions

A 3D hydrodynamic model, modified to include influences of inundated trees and floating plants, successfully simulated thermal structure in open water, flooded forest and floating plants using field

measurements of meteorological conditions in a floodplain lake. Configurations related to the presence of vegetation included reduction in wind speed and shortwave radiation, heat exchange across the water-air interface, and flow resistance induced by high vegetation drag.

Effects of inundated forest and floating plants on thermal structure and exchange flows were examined through numerical experiments with different combination of the two types of vegetation. Simulations showed that the presence of vegetation, especially inundated forest, led to stronger stratification in both open water and vegetated areas during daytime than the situation when the vegetation was not included, and that enhanced stratification persisted during nighttime. Exchange flows between open water and vegetated habitats were suppressed in the presence of flooded forest and occurred at low velocities. Exchange flows between floating plants and adjacent habitats were enhanced or reduced by the horizontal temperature gradients induced by the presence of floating plants, and can be dominated by the horizontal temperature gradient when wind speed is low. Simulations with different wind directions further confirmed that lateral exchanges among the three habitats were common in both surface and interior of the embayment as the habitats were linked by horizontal circulations at multiple depths, with directions of currents formed during daytime reversing during nighttime as wind speed declined.

The simulations expanded knowledge obtained from laboratory experiments. Compared to the configurations found in laboratory experiments, the main differences are that AEM3D simulations included competition between flows induced by wind and temperature gradients and heat absorption among plants. In particular, high heat absorption of near-surface water among floating plants can exceed reduction of incoming solar radiation by shading and lead to reversed horizontal temperature gradients. Such has not been represented in laboratory experiments. The simulations further indicated that deforestation could lead to weakened stratification, enhanced lateral exchange and shortened retention time, and highlighted the importance to include lateral and vertical exchanges when studying gas and solutes exchanges in such vegetated environments.

Future work would benefit from more accurate drag coefficients within vegetation, multiple meteorological measurements within open and vegetated areas, and inclusion of a mechanism to generate momentum transport across an open boundary to include motions induced by internal waves from outside the domain.

CRediT authorship contribution statement

Wencai Zhou: Writing – review & editing, Writing – original draft, Visualization, Validation, Software, Methodology, Formal analysis, Data curation, Conceptualization. **John M. Melack:** Writing – review & editing, Writing – original draft, Supervision, Project administration, Funding acquisition, Data curation, Conceptualization. **Sally MacIntyre:** Writing – review & editing, Methodology, Formal analysis.

Declaration of competing interest

The authors declare that they have no known competing financial interests or personal relationships that could have appeared to influence the work reported in this paper.

Data availability

Software availability is described in the manuscript. Field data are plotted in the manuscript and can be provided if requested.

Acknowledgements

Field work was supported by Ministério da Ciência Tecnologia CNPq/LBA-Edital.68/2013, processo 458036/2013–8 to B.R. Forsberg. Support for data analysis was provided by the US National Science Foundation (Division of Environmental Biology, grant number 1753856) to JMM.

Appendix A. Supplementary data

Supplementary data to this article can be found online at https://doi.org/10.1016/j.envsoft.2024.106117.

References

Amaral, J.H.F., Borges, A.V., Melack, J.M., Sarmento, H., Barbosa, P.M., Kasper, D., de Melo, M.L., Fex-Wolf, D.D., da Silva, J.S., Forsberg, B.R., 2018. Influence of plankton metabolism and mixing depth on CO_2 dynamics in an Amazon floodplain lake. Sci. Total Environ. 630, 1381–1393. https://doi.org/10.1016/j.scitotenv.2018.02.331.

Amaral, J.H.F., Melack, J.M., Barbosa, P.M., Borges, A.V., Kasper, D., Cortés, A.C., Zhou, W., MacIntyre, S., Forsberg, B.R., 2021. Inundation, hydrodynamics and vegetation influences carbon dioxide concentrations in Amazon floodplain lakes. Ecosystems. https://doi.org/10.1007/s10021-021-00692-y.

Batchelor, G.K., 1967. An Introduction to Fluid Dynamics. Cambridge Univ. Press, Cambridge.

Barbosa, P.M., Melack, J.M., Amaral, J.H.F., MacIntyre, S., Kasper, D., Cortés, A.C., Farjalla, V.F., Forsberg, B.R., 2020. Dissolved CH_4 concentrations and fluxes to the atmosphere from a tropical floodplain lake. Biogeochemistry 148, 129–151. https://doi.org/10.1007/s10533-020-00650-1.

Casulli, V., Cheng, R.T., 1992. Semi-implicit finite difference methods for three-dimensional shallow water flow. Int. J. Numer. Methods Fluid. 15, 629–648.

Coates, M.J., Patterson, J.C., 1993. Unsteady natural convection in a cavity with non-uniform absorption of radiation. J. Fluid Mech. 256, 133–161.

Coates, M.J., Ferris, J., 1994. The radiatively driven natural convection beneath a floating plant layer. Limnol. Oceanogr. 39, 1186–1194.

Dallimore, C., 2019. Three-dimensional coupled hydrodynamic-aquatic ecosystem model, AEM3D [Software]. HydroNumerics. https://www.hydronumerics.com.au/software/aquatic-ecosystem-model-3d.

Engle, D.L., Melack, J.M., Doyle, R.D., Fisher, T.R., 2008. High rates of net primary productivity and turnover for floating grasses on the Amazon floodplain: implications for aquatic respiration and regional CO_2 flux. Global Change Biol. 14, 369–381.

Hess, L.L., Melack, J.M., Affonso, A.G., Barbosa, C., Gastil-Buhl, M., Novo, E.M.L.M., 2015. Wetlands of the lowland Amazon Basin: extent, vegetative cover, and dual-season inundated area as mapped with JERS-1 Synthetic Aperture Radar. Wetlands 35, 745–756. https://doi.org/10.1007/s13157-015-0666-y.

Hodges, B.R., Imberger, J., Saggio, A., Winters, K.B., 2000. Modeling basin-scale internal waves in a stratified lake. Limnol. Oceanogr. 45, 1603–1620.

Hodges, B.R., Dallimore, C., 2019. Aquatic Ecosystem Model: AEM3D, Science Manual. Hydronumerics, Docklands, Australia.

Imberger, J., Patterson, J.C., 1981. A dynamic reservoir simulation model – DYRESM: 5. In: Fischer, H.B. (Ed.), Transport Models for Inland and Coastal Waters. Academic Press, New York, pp. 310–361.

Jellison, R.S., Melack, J.M., 1993. Meromixis in hypersaline Mono Lake, California. 1. Stratification and vertical mixing during the onset, persistence and breakdown of meromixis. Limnol. Oceanogr. 38, 1008–1019. https://doi.org/10.4319/lo.1993.38.5.1008.

Kothyari, U.C., Hayashi, K., Hashimoto, H., 2009. Drag coefficient of unsubmerged rigid vegetation stems in open channel flows. J. Hydraul. Res. 47, 691–699. https://doi.org/10.3826/jhr.2009.3283.

Leonard, B.P., 1991. The ULTIMATE conservative difference scheme applied to unsteady one-dimensional advection. Comput. Methods Appl. Mech. Eng. 88, 17–74.

Liu, Z., Chen, Y., Wu, Y., Wang, W., Li, L., 2017. Simulation of exchange flow between open water and floating vegetation using a modified RNG k-ε turbulence model. Environ. Fluid Mech. 17, 355–372. https://doi.org/10.1007/s10652-016-9489-5.

Lovestedt, C.B., Bengtsson, L., 2008. Density-driven current between reed belts and open water in a shallow lake. Water Resour. Res. 44, W10413 https://doi.org/10.1029/2008WR006949.

MacIntyre, S., Amaral, J.H.F., Barbosa, P.M., Cortés, A.C., Forsberg, B.R., Melack, J.M., 2019. Turbulence and gas transfer velocities in sheltered flooded forests of the Amazon basin. Geophys. Res. Lett. 46, 9628–9636. https://doi.org/10.1029/2019GL083948.

Monismith, S.G., 1990. Convective motions in the sidearm of a small reservoir. Limnol. Oceanogr. 35, 1676–1702.

Monismith, S.G., Hirsh, H., Batista, N., Francis, H., Egan, G., Dunbar, R.B., 2019. Flow and drag in a seagrass bed. J. Geophys. Res.:Oceans 124, 2153–2163. https://doi.org/10.1029/2018JC014862.

Monismith, S., Alnajjar, M., Daly, M., Valle-Levinson, A., Juarez, B., Fagundes, M., Bell, T., Woodson, C.B., 2022. Kelp forest drag coefficients derived from tidal flow data. Estuar. Coast. https://doi.org/10.1007/s12237-022-01098-2.

Nakayama, K., Shintani, T., Komai, K., Nakagawa, Y., Tsai, J.W., Sasaki, D., et al., 2020. Integration of submerged aquatic vegetation motion within hydrodynamic models. Water Resour. Res. 56, e2020WR027369.

Nepf, H.M., 1999. Drag, turbulence, and diffusion in flow through emergent vegetation. Water Resour. Res. 35, 479–489.

Nepf, H.M., 2012. Hydrodynamics of vegetated channels. J. Hydraul. Res. 50, 262–279. https://doi.org/10.1080/00221686.2012.696559.

Pangala, S.R., Enrich-Prast, A., Basso, L.S., Peixoto, R.B., Bastviken, D., Hornibrook, E.R. C., Gatti, L.V., Marotta, H., Calazans, L.S.B., Sakuragui, C.M., Bastos, W.R., Malm, O., Gloor, E., Miller, J.B., Gauci, V., 2017. Large emissions from floodplain trees close the Amazon methane budget. Nature 552, 230–234.

Pokorny, J., Kvet, J., 2004. Aquatic plants and lake ecosystems. In: O'Sullivan, P.E., Reynolds, C.S. (Eds.), The Lakes Handbook: Limnology and Limnetic Ecology, vol. 1. Blackwell Publishing Ltd, Oxford, pp. 309–340.

Rudorff, C.M., Melack, J.M., Bates, D.P., 2014. Flooding dynamics on the lower Amazon floodplain: 1. Hydraulic controls on water elevation, inundation extent, and river-floodplain discharge. Water Resour. Res. 50, 1–16. https://doi.org/10.1002/2013WR014091.

Sanjou, M., Okamoto, T., Nezu, I., 2017. Experimental study on fluid energy reduction through a flood protection forest. J. Flood Risk Manag. 11, e12339 https://doi.org/10.1111//jrf3.12339, 2018.

Shan, Y., Liu, C., Nepf, H.M., 2019. Comparison of drag and velocity I model mangrove forests with random and in-line tree distributions. J. Hydrol. (Wellingt. North) 568, 735–746. https://doi.org/10.1016/j.jhydrol.2018.10.0787.

Sharip, Z., Hipsey, M.R., Schooler, S.S., Hobbs, R.J., 2012. Physical circulation and spatial exchange dynamics in a shallow floodplain wetland. Int. J. Des. Nat. Ecodyn. 7, 274–291.

Spigel, R.H., Imberger, J., Rayner, K.N., 1986. Modeling the diurnal mixed layer. Limnol. Oceanogr. 31, 533–556. https://doi.org/10.4319/lo.1986.31.3.0533.

Tan, Z., Zhuang, Q., Anthony, K.W., 2015. Modeling methane emissions from arctic lakes: model development and site-level study. J. Adv. Model. Earth Syst. 7, 459–483. https://doi.org/10.1002/2014MS000344.

Tan, Z., Zhuang, Q., Shurpali, N.J., Marushchak, M.E., Biasi, C., Eugster, W., Anthony, K. W., 2017. Modeling CO_2 emissions from arctic lakes: model development and site-level study. J. Adv. Model. Earth Syst. 9, 2190–2213. https://doi.org/10.1002/2017MS001028.

Tsakiri, M., Prinos, P., 2015. Numerical simulation of thermally driven exchange flow between open water and aquatic canopies. E-Proceedings of the 36th IAHR World Congress, 28 June – 3 July, 2015, The Hague, the Netherlands.

Zhang, X., Nepf, H.M., 2008. Density-driven exchange flow between open water and an aquatic canopy. Water Resour. Res. 44, W08417 https://doi.org/10.1029/2007WR006676.

Zhang, X., Nepf, H.M., 2009. Thermally driven exhcnage flow between open water and an aquatic canopy. J. Fluid Mech. 632, 277. https://doi.org/10.1017/s0022112009006491.

Zhang, X., Nepf, H.M., 2011. Exchange flow between open water and floating vegetation. Environ. Fluid Mech. 11, 531–546. https://doi.org/10.1007/s10652-011-9213-4.